Dalton Transactions

ROYAL SOCIETY OF CHEMISTRY

COMMUNICATION

View Article Online
View Journal | View Issue

Cite this: *Dalton Trans.*, 2022, **51**, 18373

Received 19th August 2022,
Accepted 14th November 2022

DOI: 10.1039/d2dt02724k

rsc.li/dalton

The rigidity of self-assembled cofacial porphyrins influences selectivity and kinetics of oxygen reduction electrocatalysis†

Daoyang Zhang, Matthew R. Crawley, Ming Fang, Lea J. Kyle and Timothy R. Cook *

We report the electrocatalytic Oxygen Reduction Reaction on a rigid Co(II) porphyrin prism scaffold bridged by Ag(I) ions. The reactivity of this scaffold differs significantly from previous prism catalysts in that its selectivity is similar to that of monomer (~35% H_2O) yet it displays sluggish kinetics, with an order of magnitude lower k_s of ~0.5 M^{-1} s^{-1}. The deleterious cofacial effect is not simply due to metal–metal separation, which is similar to our most selective prism catalysts. Instead we conclude the structural rigidity is responsible for these differences.

Nitrogen-containing macrocycles, especially porphyrins and related compounds, have long been studied as electrocatalysts due to their biomimetic nature[1] and ability to carry out multi-electron multi-proton processes, for example the Oxygen Reduction Reaction (ORR).[2–7] An attractive feature of these complexes is their ability to carry out four-electron four-proton (4e/4H) chemistry to take O_2 to water. Although this can be challenging on monomeric systems since there are large coordination number and redox demands for 4e/4H reactivity, there are examples of effective single-metal catalysts using isocorroles.[8] It is also possible to tune the selectivity of porphyrin catalysts using pendant bases,[9] with examples of favouring 2e/2H chemistry[10] as well as 4e/4H chemistry.[11,12]

One strategy to enforce is 4e/4H chemistry to organize two porphyrins in a cofacial geometry. A classic example of this approach is the well-studied FTF4 prism which is ~99% selective for H_2O.[13] Although metal–metal separation is important, other structural and electronic elements contribute significantly to observed cofacial effects; the selectivity of a structurally related FTF6 prism drops to 31% H_2O despite being tethered through the same sites,[14] differing only by the inclusion of two additional methylene carbons in the tethers. Later on, Nocera and co-workers showed that porphyrin–porphyrin angles can affect selectivity by reporting dibenzofuran and xanthene spaced Pacman porphyrins, which possessed more rigid linkers as compared to the amide and alkyl groups of the FTF series.[15,16] In addition to selectivity, the kinetics of ORR (standard rate constants and overpotentials) are also influenced by the nature of a given cofacial geometry.

To explore these cofacial effects, we have used coordination-driven self-assembly over the past five years to generate a library of catalytically active prisms and structural analogues, including some of the most selective molecular ORR catalysts to-date.[17–19] A self-assembly approach is advantageous because it avoids the correlation between structural complexity and synthetic difficulty that is associated with traditional stepwise molecular synthesis. Thus, it has been used to construct a wide variety of metallacycles and cages with various functionalities.[20,21] We have exploited the modularity of self-assembly to include different molecular clips and nuclearities but in all our designs, dinuclear bridges span the two porphyrin sites. An interesting feature that emerged during our studies is that our four-tethered prisms twist significantly from idealized $D_{4\ h}$ symmetry, resulting in canted molecular clips and contracted M–M separations. To the extent that this motion is dynamic in solution, the metal–metal separation may differ by up to 1 nm based on crystal structures/calculations/ideal geometry measurements. Since all of four-tethered catalysts share this feature,[22] we became interested in designs that rigidify the cofacial core. A recent report by Shionoya and co-workers[23] describes the syntheses of a cofacial Zn_2(II,II) porphyrin prism (**Zn_2Ag_4 prism**) tethered by bis(bipyridyl)Ag(I) moieties which was used for host/guest chemistry but has been unexplored for catalysis. We have adapted this structure to Co(II) (**Co_2Ag_4 prism**; Fig. 1) and herein report the synthesis, characterization, and ORR activity of this rigidified design.

The synthesis of 2,2′-bipyridinyl-5-carboxylic acid followed a literature procedure.[24] The corresponding aldehyde formed from a Swern oxidation.[25] This aldehyde was then used to synthesize the free base porphyrin and subsequently Zn(II) or Co

Department of Chemistry, University at Buffalo, The State University of New York, Buffalo, New York14260, USA. E-mail: trcook@buffalo.edu

†Electronic supplementary information (ESI) available: Experimental details, NMR spectra, mass spectrometry, cyclic voltammetry, UV-vis spectra, Koutecký–Levich analysis, and computational details. See DOI: **https://doi.org/10.1039/d2dt02724k**

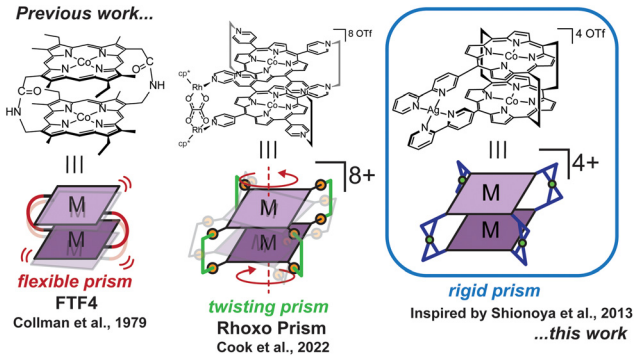

Fig. 1 Selected cofacial catalysts for ORR featuring covalently tethered architectures (FTF4), dinuclear molecular clips (Rhoxo Prism) and reported here, $Ag(bpy)_2$ metal nodes to bridge two Co(II) porphyrin building blocks.

(II) metalloporphyrins that could be self-assembled into M_2(II, II) prisms. The free-base porphyrin and Zn_2(II,II) prism[23,26] have been previously reported and the Co_2(II,II) prism is novel.

The Zn-based cofacial prism was fully characterized by ^{1}H NMR to assess symmetry and purity. The integrations matched expected values the Zn_2(II,II) cofacial stoichiometry and agreed with the literature reported values (Fig. S8†). The paramagnetic nature of the Co_2(II,II) prism makes ^{1}H NMR less informative (Fig. S9†), but there are significant differences between the electronic absorption spectra of the Co(II) porphyrin monomer and the cofacial prism. Thus, reaction progress and purity can be monitored by UV-Vis spectroscopy. The soret band of the monomeric Co(II) porphyrin is observable at λ_{max} = 416 nm and upon self-assembly this band undergoes a red-shift to λ_{max} = 433 nm (Fig. S19†). In addition, the Q-bands of the monomer appear as a single broad peak centered at 531 nm whereas these bands separate into two peaks at 551 nm and 587 nm for the prism. The stoichiometry of self-assembly can be investigated by ESI-MS, especially when clusters corresponding to intact prisms cores are identified, which is often upon the loss of counterions. We observed: m/z = 1348.9965, corresponding to $[M - 2OTf^-]^{2+}$, m/z = 1369.0182, corresponding to $[M - 2OTf^- + ACN]^{2+}$, and m/z = 863.0297, corresponding to $[M - 3OTf^- + ACN]^{3+}$ (shown in Fig. S11–13†).

The geometry of **Zn_2Ag_4** and **Co_2Ag_4 prisms** were optimized using ORCA 5.0.3.[27] The B97-3c functional and def2-mTZVP basis set were used for both the geometry optimization and the frequency calculations.[28] The prior report of **Zn_2Ag_4 prism** contains a single crystal X-ray diffraction structure that includes a guest molecule. This geometry, sans guest, was used as a starting point for optimization.[23] Our optimized structures feature M–M separation of 4.65 Å and 4.73 Å for the **Zn_2Ag_4** and **Co_2Ag_4 prisms**, respectively (Fig. 2). Furthermore, examining the displacement vectors, and vibrational modes it was found that both prisms lacks a low energy (<100 cm^{-1}) twisting mode which bring the two porphyrins together, as we discussed in our previous work.[19] We note that after multiple attempts at optimization starting from various displaced geometries, there remained a singular imaginary frequency for

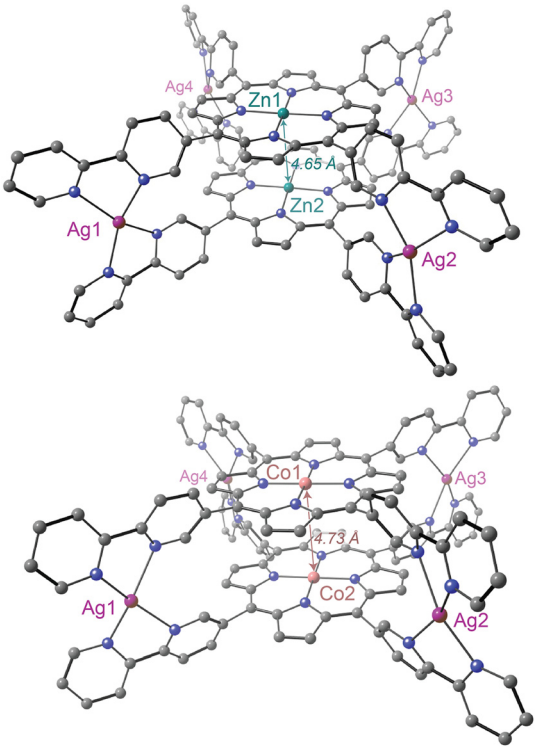

Fig. 2 Optimized structure of **Zn_2Ag_4 prism** (B97-3c with def2-mTZVP). Zn–Zn separation 4.65 Å (top); optimized structure of **Co_2Ag_4 prism** (B97-3c with def2-mTZVP). Co–Co separation 4.73 Å (bottom).

Zn_2Ag_4 and two for **Co_2Ag_4 prisms**, which corresponds to the two porphyrin macrocycles moving towards one another; however, it does not possess the twisting motion expected for more flexible cofacial prisms. Ultimately, small imaginary frequencies are not unexpected for a large molecule like these prisms. Even at the closest point in this vibration, the two metal centres are never closer than 4.4 Å. Visualization of the frontier orbitals reveals that the HOMO is primarily Ag d-orbital based for both prisms, while the LUMO is primary a Gouterman-type porphyrin centred orbital for **Zn_2Ag_4** and Co-based $d_{x^2-y^2}$ mixed with porphyrin-based atomic orbitals for **Co_2Ag_4**.

To explore the ORR reactivity of **Co_2Ag_4 prism**, cyclic voltammetry measurements were carried out under both homogeneous and heterogeneous conditions (Fig. 3). For the former, the CV shows negligible background current when O_2 is purged from the cell. When O_2 is present without a proton source, a feature consistent with reversible superoxide formation is observed with an $E_{1/2}$ of −1.28 V *vs.* Fc^+/Fc. When protons are present without an O_2 source, a catalytic wave appears at −1 V, which is associated with HER (shown in Fig. S15†). This wave is outside the window where ORR occurs in this system. When both trifluoroacetic acid and O_2 are present, a large current response (onset just below 0 V *vs.* Fc^+/Fc) is observed, consistent with data collected on our previous catalysts,[17–19,22] that we assign as catalytic O_2 reduction (Fig. 3, top). Heterogeneous CVs were measured under acidic con-

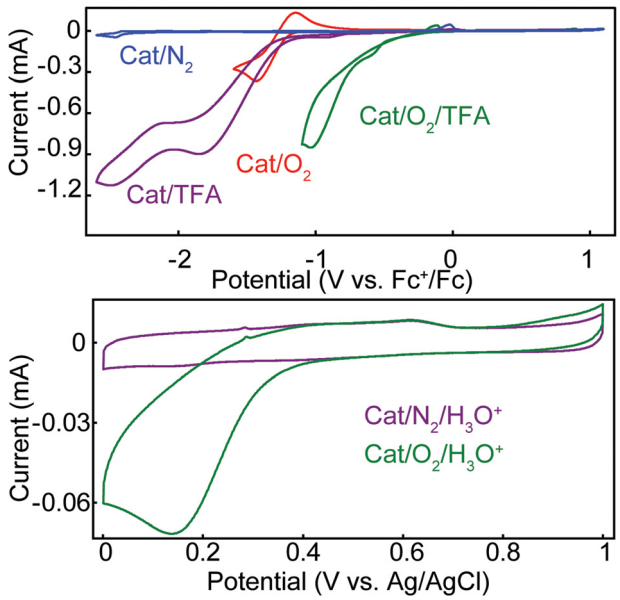

Fig. 3 (Top) CVs of **Co_2Ag_4 prism** under homogeneous conditions. 0.1 mM prism, N_2 atmosphere (blue); 0.1 mM prism, O_2 atmosphere (red); 0.1 mM prism, 100 mM TFA, N_2 atmosphere (purple); 0.1 mM prism, O_2 atmosphere, 100 mM TFA (green). All in acetonitrile with 100 mM $TBAPF_6$. Scan rate: 100 mV s^{-1}. (Bottom) heterogeneous conditions. N_2 atmosphere (purple); O_2 atmosphere (green). **Co_2Ag_4 prism** was immobilized in Nafion inks with carbon black and immersed in 0.5 M H_2SO_4. Scan rate: 100 mv s^{-1}.

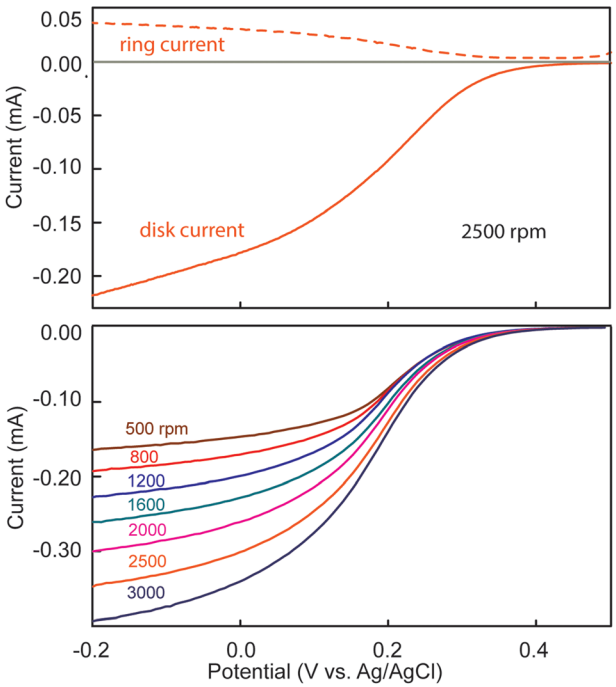

Fig. 4 (Top) Hydrodynamic voltammograms of **Co_2Ag_4 prism** at scan rates of 20 mV s^{-1}; (bottom) LSV at different rotation rates. **Co_2Ag_4 prism** was immobilized in Nafion inks with carbon black and immersed in 0.5 M H_2SO_4. The ring potential was held at 1 V.

ditions after purging with either N_2 or O_2. No proton reduction was observed when potentials were swept to 0 V *vs.*Ag/AgCl. Under acidic conditions with O_2 a catalytic response was observed, consistent with ORR mediated by our **Co_2Ag_4 prism** immobilized in an ink of carbon black and Nafion (Fig. 3, bottom).

To probe the ORR selectivity of these catalysts, rotating-ring disk electrode (RRDE) studies were performed. As with the heterogeneous CV experiments, the catalyst was immobilized in an ink of Nafion and carbon black and affixed to the glassy carbon disk. For RRDE measurements to calculate % H_2O_2, the ring and disk currents were collected at a rotation rate of 2500 rpm where both ring and disk show an appreciate current response. Fig. 4 (top) shows representative data and the ratios of these currents may be used to calculate the faradaic efficiency of H_2O_2 (see ESI eqn (S5)†). Hydrodynamic voltammetry may also be used to determine the standard rate constant for a process; as such, Koutecký–Levich analysis was conducted with the linear sweep voltammograms shown in Fig. 4 (bottom). We summarize these results along with a recently reported prism bridged by Rh-based molecular clips and CoTPyP monomer (Table 1). Our catalysts that use dinuclear molecular clips to bridge the porphyrin centers are better than monomer both in terms of selectivity and kinetics. For example, our most recently reported Co_2 Rhoxo prism is 85.5% selective for H_2O, and has a k_s value that is two orders of magnitude greater than CoTPyP. In contrast, the **Co_2Ag_4 prism** here

Table 1 Parameters of Co_2 prism inks determined by electrochemical analyses

Prism	$E_{cat/2}$ [a]	E_{onset} [a]	N_{app} [b]	% H_2O_2	%H_2O [c]	k_s [d] (M^{-1} S^{-1})
CoTPyP	0.14	0.28	2.8	61.3%	38.7%	$3.5(3) \times 10^0$
Co_2 Rhoxo	0.27	0.40	3.9	14.5%	85.5%	$2.6(2) \times 10^2$
Co_2Ag_4	0.28	0.40	2.7	65.5%	34.5%	$5.0(8) \times 10^{-1}$

[a] Potential in V *vs.* Ag/AgCl. [b] Determined based on the following equation: $N_{app} = 4 - 2\frac{(\%H_2O_2)}{100}$. [c] 100 − % H_2O_2. [d] Determined based on equation: $i_k = nFAK_{het}[O_2]\Gamma_{cat}$.

is less selective than monomer (34.5% *versus* 38.7%, respectively), and its standard rate constant is an order of magnitude lower at $5.0(8) \times 10^{-1}$ M^{-1} s^{-1} *versus* $3.5(3) \times 10^0$ M^{-1} s^{-1}.

These results are significant because the **Co_2Ag_4 prism** possesses the same cofacial geometry as many of our highly selective prisms and even shares a similar metal–metal separation. Simplistically, the cofacial enhancement is attributed to the presence of two metals at a separation that enable both to participate in key transformations that ultimately break the O–O bond to form water rather than preserving it to generate H_2O_2. That said, it is known that metal–metal separation is not the sole factor that governs selectivity and other structural elements are important. For example, when the porphyrin rings become offset, the mode by which O_2 interacts may differ resulting in a mechanistic shift. This has previously been explored by Chang and co-workers,[29] and more recently

we demonstrated this effect using self-assembly with lower-symmetry prisms.[22] The **Co_2Ag_4 prism** demonstrates that a slipping of the rings is not the only way to disrupt the e^4p^4 pathway. The bpy moieties result in more rigidity than when 4-pyridyl donors are used. We observe a twisting of the porphyrin faces when dinuclear clips are used in self-assembly. As the $D_{4\ h}$ symmetry descends to D_4, the molecular clips adopt canted arrangements but can continue to bridge between two pyridyl sites. We have observed typical porphyrin–porphyrin twists from single crystal X-ray structures. In contrast, the square-planar Ag(I) nodes of the **Co_2Ag_4 prism** cannot adopt the same canted angles. If the bpy moieties are perpendicular to the porphyrin planes, the prism possesses idealized $D_{4\ h}$ symmetry with a maximum metal–metal separation. Twisting the porphyrins away from an eclipsed geometry would break the square planar environment at the Ag(I) sites. The difference in directionality of the 4-pyridyl coordination vectors (parallel to the porphyrin plane) *versus* the chelate planes of the bpy moieties (perpendicular to the porphyrin plane) enables the former to twist, and the latter to remain essentially eclipsed.

Conclusions

We have expanded our library of self-assembled cofacial porphyrin catalysts for ORR beyond dinuclear molecular clips to include single-ion nodes between bipyridyl moieties by adapting a known Zn_2(II,II) core to a catalytically active Co_2(II,II) variant. This new prism was fully characterized and is a competent electrocatalyst for ORR. Although the metal–metal separation is similar to our previous catalysts that are highly selective for four-electron four-proton chemistry, the **Co_2Ag_4 prism** is slightly less selective than CoTPyP monomer. In addition, the standard rate constant as measured by RDE experiments is an order of magnitude lower than monomer and three orders of magnitude smaller than our prisms bridged by dinuclear clips. We rationalize these differences on the basis of structural rigidity, where the Ag(I) bpy nodes are rigid and enforce an eclipsed orientation of the porphyrin faces. These result compliments our recent findings that lower-symmetry porphyrins can significantly tune selectivity and kinetics and further highlight how the modularity of self-assembly is a power feature to design and study polynuclear catalysts based on structural tuning (metal–metal separation, stoichiometry of assembly, electronic structure, and now rigidity).

Author contributions

D. Z.: conceptualization, experimental investigation, formal analysis, writing – original draft. M. R. C.: computational investigation, formal analysis, writing – original draft. L. J. K.: electrochemical investigation. M. F.: mass spectrometry investigation. T. R. C.: conceptualization, formal analysis, funding acquisition, project administration, supervision, validation, writing – review & editing.

Conflicts of interest

There are no conflicts to declare.

Acknowledgements

This work was supported by NSF CAREER Award #1847950 (T. R. C.) and a UB Edward J. Kikta Jr Fellowship (D. Z.). D. Z. thanks Hongjia Zhou for graphic design.

References

1 N. G. Léonard, R. Dhaoui, T. Chantarojsiri and J. Y. Yang, *ACS Catal.*, 2021, **11**, 10923–10932.
2 R. Jasinski, *Nature*, 1964, **201**, 1212–1213.
3 J. Rosenthal and D. G. Nocera, *Acc. Chem. Res.*, 2007, **40**, 543–553.
4 M. L. Pegis, C. F. Wise, D. J. Martin and J. M. Mayer, *Chem. Rev.*, 2018, **118**, 2340–2391.
5 X. Li, H. Lei, L. Xie, N. Wang, W. Zhang and R. Cao, *Acc. Chem. Res.*, 2022, **55**, 878–892.
6 P. T. Smith, Y. Kim, B. P. Benke, K. Kim and C. J. Chang, *Angew. Chem., Int. Ed.*, 2020, **59**, 4902–4907.
7 Z. Liang, H. Guo, G. Zhou, K. Guo, B. Wang, H. Lei, W. Zhang, H. Zheng, U.-P. Apfel and R. Cao, *Angew. Chem., Int. Ed.*, 2021, **60**, 8472–8476.
8 Q. Cai, L. K. Tran, T. Qiu, J. W. Eddy, T.-N. Pham, G. P. A. Yap and J. Rosenthal, *Inorg. Chem.*, 2022, **61**, 5442–5451.
9 B. Lv, X. Li, K. Guo, J. Ma, Y. Wang, H. Lei, F. Wang, X. Jin, Q. Zhang, W. Zhang, R. Long, Y. Xiong, U.-P. Apfel and R. Cao, *Angew. Chem., Int. Ed.*, 2021, **60**, 12742–12746.
10 J. Yang, P. Li, X. Li, L. Xie, N. Wang, H. Lei, C. Zhang, W. Zhang, Y.-M. Lee, W. Zhang, R. Cao, S. Fukuzumi and W. Nam, *Angew. Chem., Int. Ed.*, 2022, **61**, e202208143.
11 A. Ghatak, S. Bhunia and A. Dey, *ACS Catal.*, 2020, **10**, 13136–13148.
12 R. Zhang and J. J. Warren, *J. Am. Chem. Soc.*, 2020, **142**, 13426–13434.
13 J. P. Collman, M. Marrocco, P. Denisevich, C. Koval and F. C. Anson, *J. Electroanal. Chem. Interfacial Electrochem.*, 1979, **101**, 117–122.
14 J. P. Collman, P. Denisevich, Y. Konai, M. Marrocco, C. Koval and F. C. Anson, *J. Am. Chem. Soc.*, 1980, **102**, 6027–6036.
15 C. J. Chang, Z.-H. Loh, C. Shi, F. C. Anson and D. G. Nocera, *J. Am. Chem. Soc.*, 2004, **126**, 10013–10020.
16 Y. Deng, C. J. Chang and D. G. Nocera, *J. Am. Chem. Soc.*, 2000, **122**, 410–411.
17 A. N. Oldacre, A. E. Friedman and T. R. Cook, *J. Am. Chem. Soc.*, 2017, **139**, 1424–1427.

18 A. N. Oldacre, M. R. Crawley, A. E. Friedman and T. R. Cook, *Chem. – Eur. J.*, 2018, **24**, 10984–10987.
19 M. R. Crawley, D. Zhang, A. N. Oldacre, C. M. Beavers, A. E. Friedman and T. R. Cook, *J. Am. Chem. Soc.*, 2021, **143**, 1098–1106.
20 T. R. Cook and P. J. Stang, *Chem. Rev.*, 2015, **115**, 7001–7045.
21 L. Xu, Y.-X. Wang, L.-J. Chen and H.-B. Yang, *Chem. Soc. Rev.*, 2015, **44**, 2148–2167.
22 D. Zhang, M. R. Crawley, A. N. Oldacre, L. J. Kyle, S. N. MacMillan and T. R. Cook, *Inorg. Chem.*, 2022, DOI: **10.1021/acs.inorgchem.2c01109**.
23 T. Nakamura, H. Ube and M. Shionoya, *Angew. Chem., Int. Ed.*, 2013, **52**, 12096–12100.
24 C. W. Y. Chung and P. H. Toy, *J. Comb. Chem.*, 2007, **9**, 115–120.
25 Y. Kawaguchi, S. Yasuda, A. Kaneko, Y. Oura and C. Mukai, *Angew. Chem., Int. Ed.*, 2014, **53**, 7608–7612.
26 T. Nakamura, H. Ube, M. Shiro and M. Shionoya, *Angew. Chem., Int. Ed.*, 2013, **52**, 720–723.
27 F. Neese, F. Wennmohs, U. Becker and C. Riplinger, *J. Chem. Phys.*, 2020, **152**, 224108.
28 J. G. Brandenburg, C. Bannwarth, A. Hansen and S. Grimme, *J. Chem. Phys.*, 2018, **148**, 064104.
29 H. Y. Liu, M. J. Weaver, C. B. Wang and C. K. Chang, *J. Electroanal. Chem. Interfacial Electrochem.*, 1983, **145**, 439–447.